PASJ: Publ. Astron. Soc. Japan , 1–??,

Extremely Strong ^{13}CO $J = 3 \rightarrow 2$ Line in the "Water Fountain" IRAS 16342−3814: Evidence for the Hot-Bottom Burning

Hiroshi Imai[1], Sze Ning Chong[1], Jin-Hua He[2], Jun-ichi Nakashima[3], Chih-Hao Hsia[3], Takeshi Sakai[4], Shuji Deguchi[5], and Nico Koning[6]

[1]*Graduate School of Science and Engineering, Kagoshima University, 1-21-35 Korimoto, Kagoshima 890-0065*
hiroimai@sci.kagoshima-u.ac.jp

[2]*Yunnan Astronomical Observatory/ Key Laboratory for the Structure and Evolution of Celestial Objects, Chinese Academy of Sciences, Kunming, Yunnan Province 650011, China*

[3]*Department of Physics, The University of Hong Kong, Pokfulam Road, Hong Kong, China*

[4]*Institute of Astronomy, The University of Tokyo, 2-21-1 Osawa, Mitaka, Tokyo 181-8588*

[5]*Nobeyama Radio Observatory, National Astronomical Observatory, Minamimaki, Minamisaku, Nagano 384-1305*

[6]*Department of Physics and Astronomy, University of Calgary, Calgary, AB T2N 1N4, Canada*

(Received 2011 October 22; accepted 2012 March 15)

Abstract

We observed four "water fountain" sources in the CO $J = 3 \rightarrow 2$ line emission with the Atacama Submillimeter Telescope Experiment (ASTE) 10 m telescope in 2010–2011. The water fountain sources are evolved stars that form high-velocity collimated jets traced by H_2O maser emission. The CO line was detected only from IRAS 16342−3814. The present work confirmed that the ^{12}CO to ^{13}CO line intensity ratio is ∼1.5 at the systemic velocity. We discuss the origins of the very low ^{12}CO to ^{13}CO intensity ratio, as possible evidence for the "hot-bottom burning" in an oxygen-rich star, and the CO intensity variation in IRAS 16342−3814.

Key words: stars: AGB and post-AGB — stars: individual (IRAS 16342−3814)

1. Introduction

The "water fountain" sources are a rare group of asymptotic giant branch (AGB) or post-AGB stars that show H_2O maser emission with a total velocity width larger than that typically seen in 1612 MHz OH masers. Previous radio interferometric observations have revealed that the water fountains have highly collimated, fast jets traced by H_2O maser emission while some of them still have circumstellar envelops (CSEs) as seen around AGB and post-AGB stars (Imai et al. 2002; Claussen et al. 2009; Walsh et al. 2009; Day et al. 2010, see also a review of Imai et al. 2007). It has been suggested that the dynamical ages of the jets are shorter than 100 years (Imai et al. 2007). Thus it is expected that the water fountains should shed light on the mechanism of jet launching found in planetary nebulae (PNe) and on that of the formation of asymmetric PNe (e.g. Sahai & Trauger 1998). However, because the volume of the maser emission regions is quite limited, observations of thermal emission such as CO and dust continuum are essential for understanding the whole spatio-kinematical structures of the water fountains.

He et al. (2008) and Imai et al. (2009) reported the first example of CO emission towards a water fountain source IRAS 16342−3814 (hereafter abbreviated as I16342), whose CO emission lines ($J = 2 \rightarrow 1$ and $J = 3 \rightarrow 2$ respectively) were detected in single-dish observations. The failure of CO emission detection towards other water fountains (Imai et al. 2009) may be attributed to the following factors; they are located close to the Galactic plane with heavy contamination from the interstellar CO emission, they are too distant ($D \gtrsim 2$ kpc), or the observed coordinates had large offsets from the true coordinates of the sources. Nevertheless, we can learn interesting properties of the CO emission from I16342. He et al. (2008) found a very low ^{12}CO to ^{13}CO line intensity ratio (∼1.7). The ^{12}C/^{13}C abundance ratio is not only much lower than those towards interstellar clouds (∼70, e.g., Milam et al. 2005) but also lower than other AGB/post-AGB stars (e.g., Schöier & Olofsson 2000). Imai et al. (2009) also detected high-velocity wings in the ^{12}CO $J = 3 \rightarrow 2$ spectrum, whose total velocity range is comparable to that of the H_2O maser spectrum[1].

In this paper, we report the results of additional observations of the CO $J = 3 \rightarrow 2$ lines towards I16342 with the Atacama Submillimeter Telescope Experiment (ASTE) 10 m telescope. They were conducted to reconfirm the low ^{12}CO to ^{13}CO line intensity ratio reported by He et al. (2008) but for the $J = 3 \rightarrow 2$ lines.

[1] In this paper, the CO spectrum published in Imai et al. (2009) is revised. See Sect. 3.

2. Observations and data reduction

The new ASTE observations of the CO $J = 3 \rightarrow 2$ emission were conducted during LST 16:00–22:00/20:00–22:00 on 2010 August 16/17 and LST 13:00–21:00 on 2011 June 10. In 2010, the ^{12}CO $J = 3 \rightarrow 2$ emission at 345.79599 GHz was observed towards four water fountain sources listed in Table 1. In 2011, ^{13}CO $J = 3 \rightarrow 2$ emission at 330.587957 GHz was observed towards only I16342 so as to achieve a spectral noise level roughly equal to that of ^{12}CO [2]. The FWHM beam sizes of the ASTE telescope are $22''$ and $23''$ at the observed frequencies of 345 GHz and 330 GHz, respectively. The system temperature was between 210 and 420 K (single side band). The received signals were down-converted in frequency and transferred into three (in 2010) and four (in 2011) base band channels (BBCs), each of which has a band width of 512 MHz, corresponding to a velocity width of 445 km s^{-1} at 345 GHz. In 2010, the center frequencies of the BBCs were split by 100 MHz to check the intrinsic CO emission, which should be detected in different spectral channels but at the same velocity ranges in the all BBCs[2]. In 2011, the center frequencies of the BBCs were set to the rest frequencies of ^{12}CO, ^{13}CO, C^{18}O ($J = 3 \rightarrow 2$), HCN, H^{13}CN, HC^{15}N ($J = 4 \rightarrow 3$), SO_2 (at 331.580 GHz)), CS, HCO$^+$, H^{13}CO+ ($J = 4 \rightarrow 3$), and SiC_2 (at 357.473 GHz). However, except CO, no detection was confirmed in the 3-σ upper limit to 12–16 mK. This paper reports the results of the ^{12}CO and ^{13}CO observations. We used the MAC spectrometer to obtain a spectrum with 1024 spectral channels, corresponding to a frequency and velocity spacings of 500 kHz and 0.45 km s^{-1}, respectively.

An antenna pointing check was made before every change from one target source to another. We used the CO emission towards the AGB stars II Lup and W Aql. The pointing offset derived in these measurements was always within $\sim 2''$, indicating that the pointing stability may be equal to this typical offset value in most of the observations. For antenna temperature calibration, ^{12}CO and ^{13}CO lines towards W28 were observed. Reduction of the spectral data was made using the NewStar package developed at the Nobeyama Radio Observatory.

Nine consecutive spectral channels were re-binned to a velocity resolution of 4.1 km s^{-1} to improve the signal-to-noise ratio. Comparing the antenna temperatures of the W28 CO lines with those obtained with the Caltech Submillimeter Observatory (CSO) 10 m telescope (Wang et al. 1994) and assuming an antenna aperture efficiency of ASTE ($\eta_{\rm MB}$ =0.59, Imai et al. 2009), we set conversion factors of antenna temperature scales in the BBCs. The original temperature scales were multiplied by these factors with values within a range of 1.0–1.3 to obtain the corrected scales. The emission-free baseline has a linear gradient for the integrated spectrum of IRAS 16342−3814, and it was removed to obtain the final spectrum. On the other hand, gentle standing waves can be seen in the spectra of other sources. A higher order polynomial baseline was therefore removed. The baseline removal did not affect the identification of line features in the spectra because the wavelength of the standing waves is usually much broader than a typical line width ($\Delta V \leq$50 km s^{-1}).

Table 1 gives parameters of the water fountain sources and the observations. The observations were made in the antenna-position switching mode; the number of points observed on and around the target source (>1 for the cross-scan mode) is given in Column 10. Because all the sources except IRAS 16342−3814 are located very close to the Galactic plane with intense background molecular emission, five-points or nine-points cross scans were adopted, in which the observed points were separated by $10''$–$20''$(see sect. 3). Column 11 in table 1 gives root-mean-square noise levels of the spectra.

3. Results

We searched for ^{12}CO $J = 3 \rightarrow 2$ emission towards IRAS 18043−2116 (OH 009.1−0.4), IRAS 18139−1816 (OH 12.8−0.9), and IRAS 19190+1102 with the ASTE telescope. However, after removing interstellar contamination by subtracting the off-point spectra in our cross-scans, no intrinsic CO emission could be recognized around the expected systemic velocities. The upper limit of CO $J = 3 \rightarrow 2$ emission is given by 3 times the root-mean-square noise level shown in Table 1.

Figure 1a shows the spectra of the ^{12}CO and ^{13}CO $J = 3 \rightarrow 2$ lines toward IRAS 16342−3814. To obtain these spectra with improved sensitivity in 2010, two or three MAC spectra covering different velocity ranges were synthesized[3]. The spectrum obtained in 2011 is synthesized from only the data at the source position, and shown in Figure 1a. The ^{12}CO spectra obtained in the three observations seem to be composed of two components: a wide wing ($V_{\rm LSR} \lesssim$15 km s^{-1} and $V_{\rm LSR} \gtrsim$75 km s^{-1}) and a central sharp peak ($15 \lesssim V_{\rm LSR} \lesssim 75$ [km s^{-1}]). They look roughly symmetric around the systemic velocity ($V_{\rm LSR} \simeq$45 km s^{-1}) but with some deviation as mentioned later. Although cross-scan observations were performed, the CO emission was detected only at the position of I16342 (Figure 1b). Although the emission seems to be marginally detected at the points $12''$ away from the source position, it does not mean the existence of extended components because even a perfect point source should be detected at these locations. The peak antenna temperature seems to exhibit temporal variation, whose origin is discussed in Sect. 4.3. The narrower and weaker ^{13}CO emission is also detected at the target position. The peak

[2] We tried to observe the ^{13}CO line on 2010 August 16, but the obtained data should be dropped out because later we confirmed that we observed it in a wrong frequency setup.

[3] In this step, we realized that the spectrum shown in Imai et al. (2009) was incorrectly synthesized from the spectra obtained from three BBCs. For two out of the three spectra covering different velocity ranges, the frequency scale was incorrectly converted to the velocity scale, leading to a velocity-averaged spectrum exhibiting a velocity width and a peak antenna temperature larger and less than the true ones, respectively. In this paper, the correctly synthesized spectrum is displayed.

velocities of the ^{13}CO spectrum seems to be blue-shifted from that of ^{12}CO by ∼8 km s^{-1}. Although it is difficult to judge whether this shift is real, the comparison of the ^{12}CO spectrum with the ^{13}CO one supports the shift and the asymmetry of the former relative to the latter. They may indicate the optically-thick property of the ^{12}CO line, which is discussed in Sect. 4.2.

Table 2 gives parameters of Gaussian fitting to the observed spectra in the cases assuming one and two Gaussian components. Interestingly, the ^{12}CO to ^{13}CO line intensity ratio is very low (∼1.5) at the near systemic velocity. The derived intensity ratio is roughly consistent with that for the CO $J = 2 \rightarrow 1$ lines (He et al. 2008). The ^{13}CO line has a velocity width a little larger than that of the narrow peak component of the ^{12}CO spectrum. However, it is difficult to recognize the existence of high velocity wings in the ^{13}CO spectrum.

4. Discussion

4.1. Origins of the high-/low-velocity components in the CO spectra

The ^{12}CO line profiles, as shown Figure 1, exhibit both of a narrow component ($V_{\rm exp} \lesssim$40 km s^{-1}) and very wide wings ($V_{\rm exp} \gtrsim$100 km s^{-1}). The one-Gaussian model has large deviation over the 3-σ noise level from the observed spectrum. In the case of an optically thick spherically-expanding flow as seen in CSEs of AGB stars, an observed CO emission shows a parabolic spectral profile (c.f., Kemper et al. 2003). In contrast, the ^{12}CO line profile towards I16342 resembles a Gaussian rather than parabolic shape. Taking into account the models for different opacity cases (e.g., De Beck et al. 2010), it suggests that at least the CO emission associated with the high velocity jet has a Gaussian profile and should be unresolved and optically thin. In fact, the jet and the equatorial flow should be smaller than the ASTE beam (Dijkstra et al. 2003; Sahai et al. 2005; Verhoelst et al. 2009). The existence of a central dark lane has also been confirmed in optical images (Sahai et al. 1999; Sahai et al. 2005). Therefore it is reasonable to assume that the observed CO emission in I16342 comes from both of a fast bipolar flow and a slowly expanding torus/CSE around I16342.

On the other hand, the ^{13}CO line profiles, as shown Figure 1, exhibit only a narrower component. If the both of the ^{12}CO and ^{13}CO lines have the same line profile, high-velocity wings of the latter line should also be detected over the 3-σ noise level. Actually the absence or weakening of such wing components in the latter line is recognized. If supposing a common ^{12}CO/^{13}CO abundance ratio in the whole observed region, some opacity effects should be considered to explain the difference in the ^{12}CO and ^{13}CO profiles.

Using the morpho-kinematic software *SHAPE* (Steffen & López 2006; Steffen et al. 2011), we have reproduced both the physical and kinematic structure of I16342 with a single model. To constrain the geometrical and physical parameters, we have made use of the near-infrared image of Sahai et al. (2005). They suggest the image represents light from a central star scattered by dust in dense shells surrounding a tenuous bipolar cavity. Our model therefore consists of a bipolar cavity extending 1″ on either side of the central star embedded within a spherical halo of radius $r_{\rm halo}$ =1.5″ halo. The halo contains both CO and dust and has a density profile $\rho({\rm halo}) = \rho_{0,{\rm halo}}(r/r_{0,{\rm halo}})^{-2}$ $(0 \leq r \leq r_{0,{\rm halo}})$. The surrounding cavity is a thin, dense shell of CO and dust; presumably swept up by the high velocity jet. The cavity is inclined at i =30°to the observer with a PA of 67°. The geometry of the model is displayed in Figure 2.

Using radiative transfer in *SHAPE*, to simulate the emission, absorption, and scattering for dust and the first two kinds of molecular particles with different opacities in a given temperature (see Steffen et al. 2011 for the technical details), this model produces the image displayed in Figure 3a. The model is able to reproduce the general appearance of I16342 seen in the image from Sahai et al. (2005) (Figure 3b) in scattered light including the extent of both the lobes and dark equatorial waste. To constrain the kinematics of I16342, we use the results from our current study. The CO emission in our model originates in the dense shell surrounding the cavity, and from the extended spherical halo. The velocity within the shell has the form $V_{\rm exp}$(jet) =300 km s$^{-1}[r/1'']$. Since the cavity extends out to 1″, the maximum speed of the jet is 300 km s^{-1} at the tip (c.f. Claussen et al. 2009). The spherical halo is given a constant radial velocity of 15 km s^{-1}. With these kinematic parameters and the aforementioned physical model, *SHAPE* is able to reproduce the spectra for ^{12}CO and ^{13}CO in Figure 3c and d, respectively. We find that because of the absence of high velocity wings in the latter spectrum, ^{13}CO, a tracer of higher density gas, is not bright in the high-density shell, but only in the halo. ^{12}CO, on the other hand, is bright in both the shell and the halo. This suggests that a higher intensity ratio of ^{12}CO to ^{13}CO may exist in the shell where high temperatures (>600K, see Sect. 4.2) are expected and H_2O and OH maser actions are excited.

4.2. Extremely low ^{12}CO to ^{13}CO intensity ratio

We confirmed a very low ^{12}CO/^{13}CO line intensity ratio (∼1.5) for the $J = 3 \rightarrow 2$ and $J = 2 \rightarrow 1$ (He et al. 2008) transitions towards I16342. At first, one may suppose that this is attributed to an opacity effect of these lines. To examine such a possibility, in other words whether even a typical ^{12}CO/^{13}CO abundance ratio as seen in interstellar clouds (∼70, e.g., Milam et al. 2005) can explain such a low line intensity ratio, we performed another radiative-transfer simulations that repeatedly calculated the line opacities and the line intensity ratio. Note that *SHAPE* does not constrain CO line opacities properly because a line opacity in it is manually tuned to reproduce the observed brightness distribution of the line/continuum emission from the morpho-kinematical model. Thus we resort to another radiative transfer code *RADEX* [1] (Van der Tak et al. 2007), which makes use

[1] http://www.strw.leidenuniv.nl/~moldata/radex.html

the molecular line database *LAMDA* (Schöier et al. 2005) and treats the radiative transfer and CO rotational level excitation in a self-consistent way. After many trials with changing input physical parameters such as volume density (10^2 cm^{-3} $< n_{\rm H_2} \leq 10^6$ cm^{-3}), column density (10^{12} cm^{-2} $< N_{\rm CO} \leq 10^{18}$ cm^{-2}), and kinematic temperature (10 K$< T_{\rm k} \leq$1000 K), the results of the calculations are summarized as follows. Here one assumes a velocity width of $\Delta V \simeq$10 km s^{-1} and $N_{\rm CO}/N_{\rm H_2} \simeq 10^{-4}$. In the case of I16342, the spectral energy distribution (SED) indicates a blackbody temperature of the CSE around $T \simeq$130 K, which was derived from fitting of a single temperature SED to the data of IRAS[2], MSX6C[3], and AKARI[4] Point Source Catalogs. Taking into account the size of the mid-infrared emission (Verhoelst et al. 2009) and the present ASTE observations, which gives an upper limit to the source size comparable to the ASTE beam size ($<20''$, the CSE/jet may have a size in the range of 6,000–10,000 AU.

First, in the case of the volume density of hydrogen molecules close to the critical value, $n_{\rm H_2} \simeq 2 \times 10^5$ cm^{-3}, the CO $J = 3 \rightarrow 2$ lines become optically thick ($\tau \simeq 1$) in a cloud with $N_{\rm CO} \gtrsim 2 \times 10^{17}$cm^{-2} or $T_{\rm k} \gtrsim$550 K. The former threshold value corresponds to a cloud size of $\sim$1000 AU and a mass loss rate of $\sim 3 \times 10^{-5} M_\odot$yr^{-1}. For the CSE of I16342 with the larger size and the higher temperature as mentioned above, the ^{13}CO opacity is estimated to be comparable to or lower than unity. On the other hand, the ^{12}CO emission has a lower critical density and may have a larger distribution including the jet, therefore, the emitting region of the ^{12}CO line may have a lower temperature and the ^{12}CO line may be optically thick. This is consistent with the assumption of such opacity difference from our *SHAPE* simulation (see Sect. 4.1). Second, the ^{12}CO/^{13}CO line intensity ratio may have the observed small value *only* in the case where $T <$20 K or $T >$550 K. Note that such low and high temperatures may appear, respectively, in the outer boundary of a CSE with a volume density lower than expected to excite the CO $J = 3 \rightarrow 2$ emission and at the innermost part of a CSE (e.g., within 100 stellar radii, Cooke & Elitzur 1985). Although tiny clumps to excite H_2O and OH maser meet such a physical condition, their volume fraction in the CSE should be extremely limited. Regardless, these temperature regions should be uncommon in the CSE. Third, in the physical conditions expected for the CSE of I16342, even if the ^{12}CO line is optically thick, a CO column density of $N_{\rm CO} > 10^{19}$ cm^{-2} is necessary to explain the observed intensity ratio if the CSE has a ^{12}CO/^{13}CO abundance ratio as seen in interstellar clouds ($\sim$70). For a moderate value ($N_{\rm CO} \lesssim 10^{18}$ cm^{-2}), a much lower abundance ratio, 4 or lower, is required. These results support, the extremely low ^{12}CO/^{13}CO abundance ratio in the CSE.

Applying a frequency correction described in Equation 15 of De Beck et al. (2010), we derive a ^{12}C/^{13}C isotopic ratio of $\sim$1.3. Such an extremely low isotopic ratio has also been confirmed in J-type carbon-rich stars (Abia & Isern 2000; Olofsson & Nyman 1999). The J-type star has a lower stellar mass ($M_* \simeq$2–3$M_\odot$) and the "cold-bottom processing" is expected, in which production of ^{13}C is enhanced, but not O (e.g., Abia & Isern 2000). On the other hand, an oxygen-rich star has a higher mass ($4M_\odot \lesssim M_* \lesssim 7M_\odot$) and the "hot-bottom burning" (HBB) is expected, in which production of both ^{13}C and O is enhanced so that ^{12}C is converted to these nucleons (see e.g. a review of Herwig 2005; De Beck et al. 2010). Therefore, the enhancement of ^{13}CO relative to ^{12}CO observed in O-rich stars should provide direct evidence for HBB in the AGB nucleosynthesis. The present results towards I16342, that clearly has O-rich chemistry harboring H_2O and OH masers, may provide one of the most clear examples of the HBB signature. Some pre-planetary nebulae with O-rich chemistry show similar cases and their progenitors are also suggested to be massive post-AGB stars (see also e.g., Nakashima et al. 2004; Nakashima et al. 2006; Dinh-V-Trung 2009). Based on the stellar luminosity and the orbit in the Galaxy, it has been demonstrated that the water fountains should harbor intermediate-mass O-rich evolved stars such as OH/IR stars and their posterity (e.g., Imai et al. 2002; Imai et al. 2007; Imai 2007). The possibility of HBB is consistent with this view. Direct determination of the original mass of the central star of I16342 is a future issue in theoretical and observational works.

4.3. Temporal variation of the CO profile

In general it is difficult to precisely compare the peak (main beam) antenna temperatures, $T_{\rm MB}$, found in different observation epochs. In the present observations, the peak value of $T_{\rm MB}$ is apparently enhanced by a factor of $\sim$1.6 from the first to second epoch spectrum. Note that these $T_{\rm MB}$ scales had been corrected by using the different flux calibrators (IRC+10216 in 2008 and W28 in 2010 and 2011, respectively) while the scaling correction factors were smaller than 1.3 in the spectrum calibration of the whole observations. It has been expected that the flux calibrators provide $T_{\rm MB}$ scales with uncertainty of $\sim$20% (e.g. Wang et al. 1994). It has not yet been reported that these calibrator spectra are variable. Therefore the intrinsic temporal variation of the I16342 CO spectrum cannot be ruled out.

However, we note that when the $T_{\rm MB}$ values are set to equal among the observations, the rescaled spectral profiles resemble each other in the whole velocity range within rms noise levels. Figure 1c displays the ^{12}CO spectra obtained in 2008 June (Imai et al. 2009), 2010 August, and 2011 June. For comparison of the whole spectra, the spectra in 2008 and 2011 are rescaled by factors of 1.6 and 1.3, respectively. As discussed in Sect. 4.1, the CO emission may originate from both the fast jet and the slowly expanding CSE/torus, which should be physically independent. Taking into account a possible time scale of flux variation due to discontinuous stellar mass loss or episodic events for mass eruption as well as large physical sizes of the CO sources (>1000 AU), it is difficult to ex-

[2] Infrared Astronomical Satellite, http://irsa.ipac.caltech.edu/data/download/IRAS/iras_psc.tbl
[3] Midcourse Space Experiment, http://irsa.ipac.caltech.edu/data/MSX/docs/MSX_psc_es.pdf
[4] http://darts.isas.jaxa.jp/astro/akari/cas.html

plain the $T_{\rm MB}$ variation by intrinsic temporary variation. Alternatively, different antenna pointing offsets in the observations are expected to explain the similarity of the CO spectral profiles and the different antenna temperature scales. If the CO region is an ideal point source, such a large variation cannot be expected because the pointing offsets should be much smaller than the beam size ($\lesssim 5''$). A simple Monte-Carlo simulation which decreased the antenna temperature scale suggested that, for the ASTE's beam ($22''$), the source size should be larger than $5''$(when assuming a point-symmetric, Gaussian brightness distribution) to reproduce the observed scale decrease. Figure 1b shows the spectra obtained from five-point scans conducted in 2011. The CO emission was detected only on the on-source point and the peak values of $T_{\rm MB}$ at the off-point positions are ∼40% of that at the on-source point or lower. This indicates that the angular size of the CO emission, at least the low velocity component, should be smaller than $\sim 10''$. The true angular scale of the observed CO emission is easily measured by future interferometric observations.

4.4. Mass loss rate of IRAS 16342−3814

In this paper, we reestimate a mass loss rate of the I16342 CO $J = 3 \rightarrow 2$ outflow from the revised ^{12}CO profile. With assumption of unresolved, optically thick CO emission, as mentioned in Sect. 4.2, we can derive a mass loss rate in units of solar masses per year using the formula as follows (Ramstedt et al. 2008, see also Knapp & Morris 1985; Olofsson et al. 1993; Groenewegen et al. 1999; De Beck et al. 2010),

$$\dot{M} = s_J \left(I_{\rm CO} B^2 D^2 \right)^{a_J} V_{\rm exp}^{b_J} f_{\rm CO}^{-c_J}. \quad (1)$$

Here $I_{\rm CO}$ is the velocity-integrated antenna temperature of the CO emission in K km s^{-1}, $V_{\rm exp}$ the expansion velocity of the CO emission in km s^{-1}, D the source distance in kpc, B the beam size of the telescope in arcsec, $f_{\rm CO}$ the abundance of CO molecules relative to H_2, and $s_J \simeq 3.8 \times 10^{-11}$ a correction factor for $J \rightarrow J-1$ transition, and $a_J \simeq 0.91$, $b_J \simeq 0.39$, $c_J \simeq 0.45$ the coefficients derived for $J = 3 \rightarrow 2$, respectively. For I16342, D =2 kpc and is adopted. For ASTE, B =22″ is adopted. For an O-rich circumstellar envelope harboring H_2O and OH maser emission, $f_{\rm CO} \sim 10^{-4}$ is adopted. Using the Gaussian profile parameters listed in Table 2 (here $V_{\rm exp} \simeq \Delta V_{\rm HWHM}$), the contributions to the mass loss rates from the broad-wing and the central-peak components are calculated to be $\dot{M} \simeq 4.8 \times 10^{-5} M_\odot {\rm yr}^{-1}$ and $\dot{M} \simeq 3.8 \times 10^{-6} M_\odot {\rm yr}^{-1}$, respectively. The former value is much smaller than estimated with mid-IR emission ($\dot{M}_{\rm gas} \approx 10^{-3}\, M_\odot$ yr^{-1}, Dijkstra et al. 2003) but indicates a major contribution to the total mass loss rate of I16342. However, the CO emission contribution from the former component should be more carefully examined by high resolution mapping.

5. Conclusions

Through a series of our ASTE observations, we detected the intrinsic CO emission from one source, I16342, out of 13 water fountain sources. We find a very low ^{12}CO to ^{13}CO line intensity ratio (∼1.5). This may indicate an intrinsic property of the CO emission towards the water fountain and indicates the presence of "hot-bottom burning" in the stellar nucleosynthesis. Based on arguments from e.g. Imai et al. (2007), the present results support that I16342 should be an oxygen-rich star with a mass of $4 M_\odot \lesssim M_* \lesssim 7 M_\odot$. I16342 may have a mass loss rate of $\dot{M}_{\rm gas} > 5 \times 10^{-5}\, M_\odot$ yr^{-1}. The detection of the high-velocity wings in the ^{12}CO spectrum implies a possibility that the bipolar high-velocity jet plays a major role of final stellar mass loss. High angular resolution and sensitivity CO mapping observations as those conduced with the Atacama Large Millimeter-submillimeter Array (ALMA) should dramatically increase the number of CO sources towards the water fountains within a few kilo parsecs with moderate mass loss rates as AGB stars ($> 10^{-6} M_\odot {\rm yr}^{-1}$) and spatially resolve the high-velocity wing components in the CO spectra.

We deeply appreciate members of the ASTE team for their careful observations, preparation and kind operation support. The ASTE project is driven by Nobeyama Radio Observatory (NRO), a branch of National Astronomical Observatory of Japan (NAOJ), in collaboration with University of Chile, and Japanese institutes including University of Tokyo, Nagoya University, Osaka Prefecture University, Ibaraki University, and Hokkaido University. Observations with ASTE were in part carried out remotely from Japan by using NTT's GEMnet2 and its partner R&E (Research and Education) networks, which are based on AccessNova collaboration of University of Chile, NTT Laboratories, and NAOJ. We thank T. Minamidani and H. Izumiura for introducing the radiative transfer calculation code (RADEX) and for giving fruitful comments on our work, respectively. HI and SD have been financially supported by Grant-in-Aid for Scientific Research from Japan Society for Promotion Science (20540234). JN is supported by a grant from the Research Grants Council of Hong Kong (project code: HKU 704209P; HKU 704710P; HKU 704411P) and by the financial support from the Small Project Funding of HKU (project code: 201007176004).

References

Abia, C., & Isern, J. 2000, Mem., S. A. It., 71, 631
Boboltz, D. A., & Marvel, K. B. 2007, ApJ, 665, 680
Claussen, M., Sahai, R., & Morris, M. R. 2009, ApJ, 691, 219
Cooke, B., & Elitzur, M. 1985, ApJ, 295, 175
Day, F. M., Pihlström, Y. M., Claussen, M. J., & Sahai, R. 2010, ApJ, 713, 986
De Beck, E., Decin, L., de Koter, A., Justtanont, K., Verhoelst, T., Kemper, F., & Menten, K. M. 2010, A&A, 523, A18
Deacon, R. M., Chapman, J. M., Green, A. J., & Sevenster, M. N. 2007, ApJ, 658, 1096
Deguchi, S., Nakashima, J, Kwok, S., & Koning, N. 2007, ApJ, 664, 1130

Dijkstra, C., Waters, L. B. F. M., Kemper, F., Min, M., Matsuura, M., Zijlstra, A., de Koter, A., & Dominik, C. 2003, A&A, 399, 1037
Dinh-V-Trung 2009, ApJ, 692, 1382
Groenewegen, M. A. T., F.Baas, F., Blommaert, J. A. D. L., Stehle, R., Josselin, E., & Tilanus, R. P. J. 1999, A&AS, 140, 197
He, J.-H., Imai, H., Hasegawa, T. I., Campbell, S. W., & Nakashima, J. 2008, A&A, 488, L21
Herwig, F. 2005, ARA&A, 43, 435
Huggins, P. J., 2007, ApJ, 663, 342
Imai, H., He, J.-H., Nakashima, J., Ukita, N., Deguchi, S., & Koning, N. 2009, PASJ, 61, 1365
Imai, H., Sahai, R., & Morris, M. 2007, ApJ, 669, 424
Imai, H. 2007, in: IAU Symposium 242, Astrophysical Masers and their Environments, Baan, W., & Chapman, J. (Cambridge University Press: Cambridge), p279
Imai, H., Nakashima, J., Diamond, P. J., Miyazaki, A., & Deguchi, S. 2005 ApJ, 622, L125
Imai, H., Obara, K., Diamond, P. J., Omodaka, T., & Sasao, T. 2002, Nature, 417, 829
Kemper, F., Stark, R., Justtanont, K., de Koter, A., Tielens, A. G. G. M., Waters, L. B. F. M., Cami, J., & Dijkstra, C. 2003, A&A, 407, 609
Knapp G.R., Young K., Lee E., & Jorissen A. 1998, ApJS, 117, 209
Knapp, G. R. & Morris, M. 1985, ApJ, 292, 640
Milam, S. N., Savage, C., Brewster, M. A., Ziurys, L. M., & Wyckoff, S. 2005, ApJ, 634, 1126
Nakashima, J., & Deguchi, S. 2006, ApJ, 633, 282
Nakashima, J., Deguchi, S., & Kuno, N. 2004, PASJ, 56, 193
Olofsson, H., & Nyman, L.-Å. 1999, A&A, 347, 194
Olofsson, H., Eriksson, K., Gustafsson, B., & Carlström, U. 1993, ApJS, 87, 267
Ramstedt, S., Schöier, F. L., Olofsson, H., & Lundgren, A. A. 2008, A&Ap, 487, 645
Sahai, R., Le Mignant, D., Sánchez Contreras, C., Campbell, R. D., & Chaffee, F. H. 2005, ApJ, 622, L53
Sahai, R., te Lintel Hellert, P., Morris, M., Zijlstra, A., & Likkel, L. 1999, ApJ, 514, L115
Sahai, R., & Trauger, J. 1998, AJ, 116, 1357
Schöier, F. L., van der Tak, F. F. S., van Dishoeck, E. F., & Black, J. H. 2005, A&A, 432, 369
Schöier, F. L., & Olofsson, H. 2000, A&A, 359, 586
Steffen, W., Koning, N., Wenger, S., Morisset, C., & Magnor, M. 2011 IEEE Transactions on Visulisation and Computer Graphics, 17, 454 (arXiv1003.2012S)
Steffen, W., & López, J. A. 2006, RMxAA, 42, 99
Suárez, O., Gómez, J. F., Miranda, L. F., Torrelles, J. M., Gómez, Y., Anglada, G., & Morata, O. 2009, A&A, 505, 217
Suárez, O., Gómez, J. F., & Miranda, L. F. 2008, ApJ, 689, 430
Suárez, O., Gómez, J. F., & Morata, O. 2007, A&A, 467, 1085
Van der Tak, F. F. S., Black, J. H., Schöier, F. L., Jansen, D. J., & van Dishoeck, E. F. 2007, A&A, 468, 627
Verhoelst, T., Waters, L. B. F. M., Verhoeff, A., Dijkstra, C., van Winckel, H., Pel, J. W., & Peletier, R. F. 2009, A&A, 503, 837
Walsh, A. J., Breen, S. L., Bains, I., & Vlemmings, W. H. T. 2009, MNRAS, 394, 70
Wang, Y., Jaffe, D. T., Gref, U. U., & Evans II, N. 1994, ApJS, 95, 503

Table 1. Parameters of the water fountain sources and the ASTE observations in ^{12}CO emission.

IRAS name Other name	R.A. (J2000.0) Decl. (J2000)	Year of observation	l[1] ($''$)	$V_{\rm sys}$[2] (km s^{-1})	$\Delta V_{\rm los}$[3] (km s^{-1})	D[4] (kpc)	$t_{\rm jet}$[5] (year)	Ref.[6]	Dur[7] (hr)	On-[8] point	rms (mK)
16342−3814	$16^h37^m39^s.91$	2010	2.4	50	240	2.0	100	2, 5	0.5	1	5
OH 344.1+5.8	$-38°20'17''.3$	2011							2.4	5	7
18043−2116	$18^h07^m20^s.85$	2010	0.3	87	400	6.4	60	3, 7	1.25	5	6
OH 009.1−0.4	$-21°16'12''.0$										
18139−1816	$18^h16^m49^s.23$	2010	0.12	56	50	∼8	90	1	2.25	5	6
OH 12.8−0.9	$-18°15'01''.8$										
19190+1102	$19^h21^m25^s.09$	2010	0.28	28	130	8.6	60	4, 6	0.58	5	9
	$+11°08'41''.0$								1.08	9	21

[1]Total angular length of the jet system.
[2]Systemic velocity of the jet system.
[3]Full range of the line-of-sight velocities of H_2O maser emission.
[4]Distance to the source.
[5]Dynamical age of the jet ($\approx l/\Delta V_{\rm los}$).
[6]References of the jet parameters. 1: Boboltz & Marvel (2007); 2: Claussen et al. (2009); 3: Deacon et al. (2007); 4 Day et al. (2010); 5: Imai et al. (2009); 6: Suárez et al. (2008); 7: Walsh et al. (2009).
[7]Duration of the total observation time with ASTE.
[8]Number of points observed on and around the target, except an off-point.

Table 2. Parameters of Gaussian fitting to ^{12}CO and ^{13}CO emission toward IRAS 16342−3814.

	Single Gaussian fitting			Two Gaussian fitting					
				Broad wing			Narrow peak		
Molecule	$T_{\rm MB}^{\rm peak}$ (mK)	$V_{\rm sys}$ (km s^{-1})	$\Delta V_{\rm HWHM}$ (km s^{-1})	$T_{\rm MB}^{\rm peak}$ (mK)	$V_{\rm sys}$ (km s^{-1})	$\Delta V_{\rm HWHM}$ (km s^{-1})	$T_{\rm MB}^{\rm peak}$ (mK)	$V_{\rm sys}$ (km s^{-1})	$\Delta V_{\rm HWHM}$ (km s^{-1})
^{12}CO (in 2008)[1]	37±1	47±1	59±2	23±2	46±3	105±9	26±3	46±1	23±3
^{12}CO (in 2010)	58±3	49±2	47±3	45±3	49±2	71±4	40±6	46±1	9±2
^{12}CO (in 2011)	48±2	52±2	42±3	32±3	56±3	70±6	33±5	48±1	15±3
^{13}CO (in 2011)	36±3	44±1	36±3	...	...	...	...	...	...

[1]Observed on 2008 June 20–21 (Imai et al. 2009). The spectral synthesis shown in that paper is corrected.

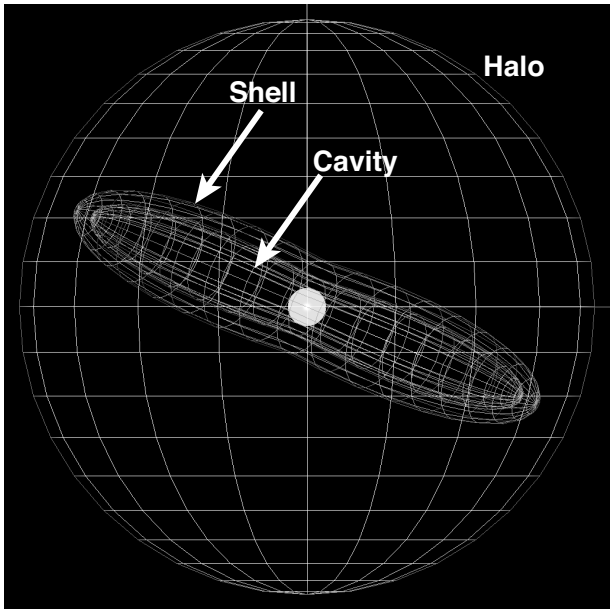

Fig. 2. *Shape* model of IRAS 16342−3814 consisting of a bipolar cavity embedded within a spherical halo of CO and dust. Surrounding the cavity is a thin dense shell which represents material swept up by the jet. The inclination of the cavity/shell is $i = 30°$.

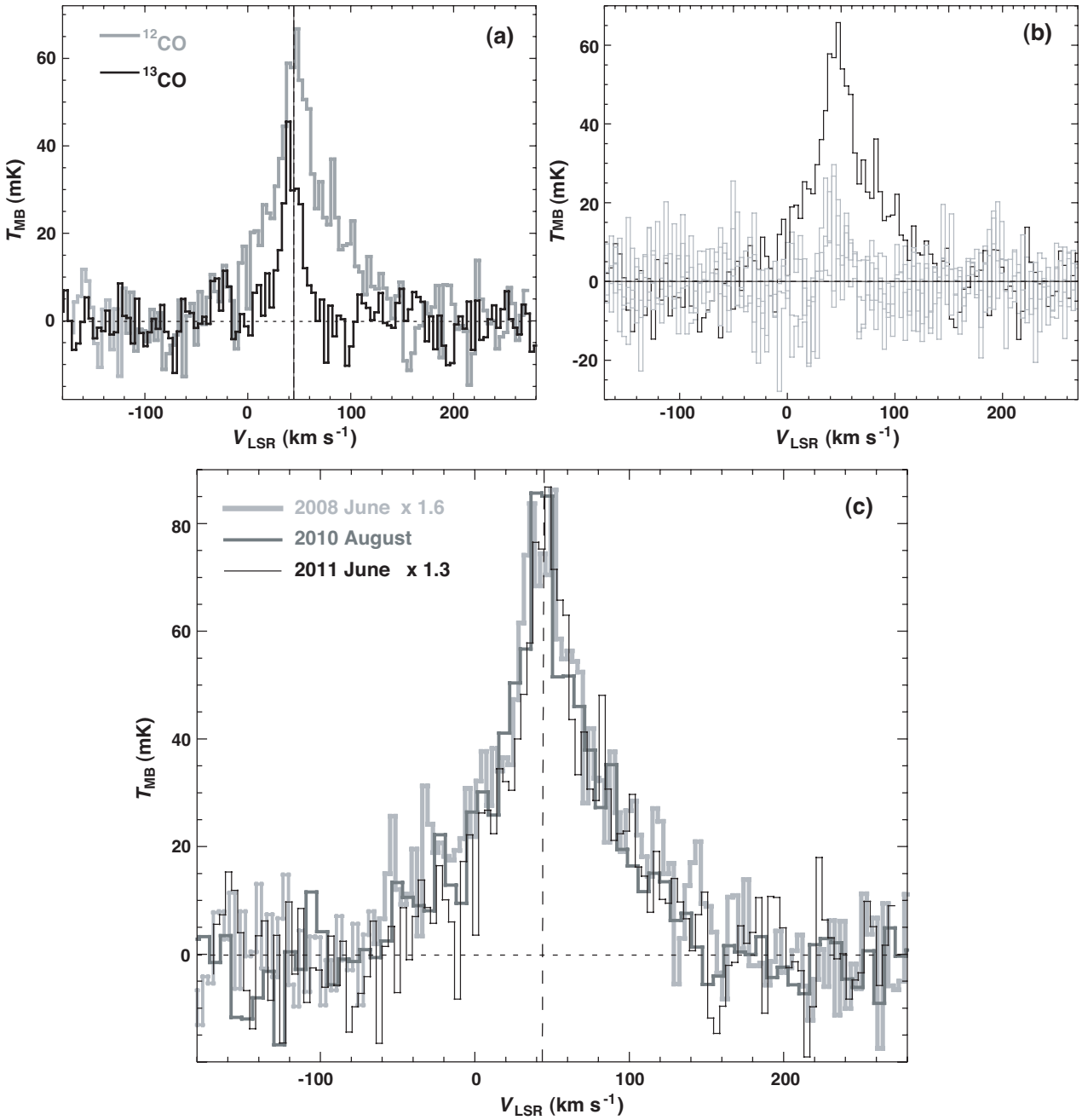

Fig. 1. Spectra of the CO $J = 3 \rightarrow 2$ emission lines toward IRAS 16342−3814. (a) The spectra of the ^{12}CO (a grey thick line) and the ^{13}CO (a black thin line) emission lines obtained in 2011 June. (b) The spectra of ^{12}CO at the source position (a black line) and the four offset positions (gray lines) in the cross-scans conducted in 2011 June. The separation between the on-source and offset positions was set to 11″ and one of the cross arms was in the direction of the major axis of the I16342 jet. (c) The ^{12}CO spectra obtained in 2008 June (a thick grey line, modified from Imai et al. 2009 and rescaled by a factor of 1.6), in 2010 August (a thick black line), and in 2011 June (a thin black line, rescaled by a factor of 1.3). The horizontal grey dashed line shows the zero-temperature baseline.

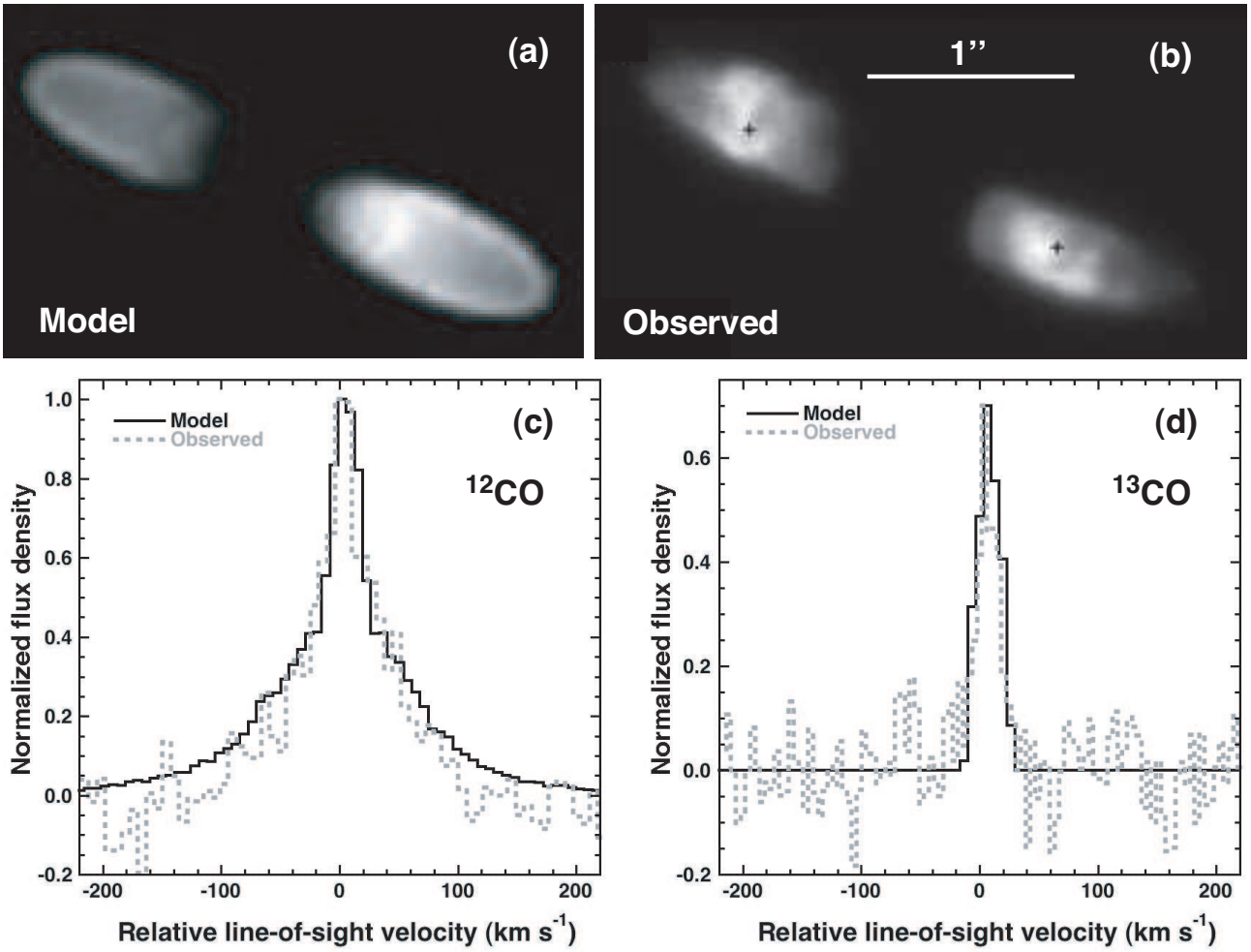

Fig. 3. Results from the *SHAPE* model compared with observations. (a) *SHAPE* rendering of the optical image model of IRAS 16342−3814. The image is created using radiative transfer within *SHAPE*. (b) Near-infrared image of IRAS 16342−3814 cited from Sahai et al. (2005). The image consists of light scattered off dust in the high density shells surrounding a tenuous interior. (c) Comparison between the observed ^{12}CO spectrum (grey dashed line) and that produced from the model (solid black line). (d) Comparison between the observed ^{13}CO spectrum (grey dashed) and that produced from the model (solid black).